

Photothermal deflection spectroscopy of an aqueous sample in a narrow bore quartz capillary

Jonathan D. Spear^{a)}

Energy and Environmental Technologies Division, Lawrence Berkeley National Laboratory, M/S 70-193A, Berkeley, California 94720

Gregory L. Klunder

Forensic Science Center, P.O. Box 808 L-178, Lawrence Livermore National Laboratory, Livermore, California 94550

Richard E. Russo

Energy and Environmental Technologies Division, Lawrence Berkeley National Laboratory, M/S 70-193A, Berkeley, California 94720 and Forensic Science Center, P.O. Box 808 L-178, Lawrence Livermore National Laboratory, Livermore, California 94550

(Received 3 March 1998; accepted for publication 24 March 1998)

An apparatus to perform photothermal deflection spectroscopy on liquid samples within a cylindrical capillary is described. A tunable dye laser, modulated by an optical chopper, serves as an excitation source. The resolution of a spectral absorption peak near 575 nm, of a 1×10^{-3} M Nd^{3+} aqueous solution, demonstrates the effectiveness of the system. The sample is contained within a 75 μm internal diameter quartz capillary, typical of those used for capillary electrophoresis. Across the middle of the probed section of the capillary, the magnitude of the resolved peak is 5.2×10^{-5} absorbance units. A helium–neon laser, focused to a $1/e^2$ waist diameter of 40 μm , provides an optical probe beam across the center of the sample, overlapping the excitation beam at an angle of 3° . Maximum signal-to-noise ratio is achieved with the apparatus when the excitation beam is modulated at a frequency near 205 Hz. The deflection responsivity of the probe beam at this frequency is 650 nrad per μW of absorbed excitation radiation, with an internal noise level in the system of 0.6 nrad $\text{Hz}^{-1/2}$. The shot noise from probe beam radiation upon the photodiodes in the position sensitive detector exceeds noise from other sources. [S0034-6748(98)03506-0]

I. INTRODUCTION

Photothermal deflection spectroscopy (PDS) is an analytical technique suitable for measuring small values of optical absorption in transparent matter.^{1–3} PDS has also been called, “mirage effect spectroscopy,” or “optothermal beam deflection spectroscopy.” Unlike conventional spectrophotometry, which measures the transmittance of a sample to an optical beam, photothermal methods⁴ such as PDS monitor temperature fluctuations due to optical radiation that the sample absorbs and converts into heat. For trace detection of an analyte in a medium that has a low optical absorption coefficient at the detection wavelength, spectrophotometry requires measurement of a small change superposed upon a relatively large background transmittance signal. Because signal drift and noise can cause problems in this situation, photothermal methods that use a high power excitation source may be preferable to spectrophotometry.

In “collinear” PDS, an optical excitation beam passes through the sample adjacent to an optical probe beam. Because the two beams are slightly offset, their axes are not exactly collinear and may not even be parallel. Absorption of the excitation beam produces small thermal gradients in the region through which the probe beam passes. Refractive index gradients accompany these thermal gradients, causing

the probe beam to be spatially deflected, and the amplitude of this deflection is monitored as a measure of radiative absorption at the excitation wavelength. Typically, the focused Gaussian output beam from a helium–neon laser serves as the optical probe, and a solid state position sensitive detector measures its deflection. The excitation beam originates from either a periodically pulsed laser or a modulated continuous-wave laser. This periodic modulation allows synchronized electronic equipment, such as a boxcar averager or a lock-in amplifier, to filter noise from the signal. In typical aqueous PDS experiments, a 1 cm spectrophotometer cuvette with flat windows contains the sample.

With the development of capillary electrophoresis (CE)^{5–8} as a separation technique for aqueous samples, interest has been shown in applying various photothermal methods to enhance detection capabilities. In capillary electrophoresis, a liquid sample is introduced into one end of a long (~ 20 – 100 cm), narrow (~ 25 – 200 μm i.d.), hollow cylindrical capillary, along which a voltage is applied. Separation occurs because the dissolved ions in the liquid migrate at different rates through the capillary. It is desirable to be able to detect the ions *in situ* as they pass through a “window” section near the distal end of the capillary. In one type of photothermal refractive index detector,^{9–11} a probe beam is directed through the capillary, near the edge of the internal

^{a)}Electronic mail: jdspear@LBL.gov

bore, and internal reflections create a pattern of light and dark fringes in the transmitted beam. Optical absorption by the fluid in the capillary causes the refractive index to change, thereby perturbing the fringe pattern. In another system, crossed-beam thermal lensing has been demonstrated,^{12,13} in which the three axes of an excitation beam, a probe beam, and a capillary, intersect perpendicularly at a single point. Absorption of the excitation beam within the capillary causes defocusing of the probe beam, which is monitored by a single photodiode. Additionally, photoacoustic experiments have been performed on a capillary segment held in mechanical tension between two fixed points, and optically excited by a beam that is modulated at the resonant vibrational frequency of the capillary segment. Either a photodiode^{14,15} or a piezoelectric transducer¹⁶ can detect the mechanical vibrations of the capillary.

The goal of the research described here was to develop and evaluate the capability of photothermal deflection spectroscopy as a detector for CE. We designed a collinear PDS apparatus that accommodates a microbore fused silica capillary to hold the sample. Instead of incorporating electrophoretic separation into our tests, we injected a dilute solution of Nd^{3+} ions into a capillary, held it stationary, and spectrally resolved its optical absorption peak. Minimizing noise was especially important, because the short path length across the capillary dictated that the deflection amplitude would be small. By observing signal and noise, we identified the capabilities and limitations of the system.

II. APPARATUS

Figures 1(a) and 1(b) show the system that was developed for this work. A Spectra-Physics model 171 argon-ion laser pumps a tunable Coherent Model CR-599 dye laser with rhodamine 560 dye to provide the optical excitation radiation. A Stanford Research Systems Model SR540 mechanical chopper, inserted between the ion laser and the dye laser, modulates the power of the excitation beam. The reason for placing the chopper between the two lasers rather than after the dye laser is to prevent scattered probe beam radiation from passing back through the chopper, reflecting off the dye laser output mirror, and then entering the system again. Although such scattered probe beam radiation would be of very low power, it would be modulated at the same frequency as the excitation beam, and therefore could interfere with the deflection measurements. Two mirrors, M_1 and M_2 , mounted on tilt plates, direct the excitation beam into a wooden enclosure. The primary purpose of the enclosure is to restrict unwanted laboratory air currents from deflecting the optical probe beam, which originates from a Uniphase Model 1303 P helium–neon laser, with an output power of 2.0 mW, a wavelength of 632.8 nm, and an initial $1/e^2$ diameter of 630 μm . Two lenses, L_1 ($f_1 = -50.8$ mm) and L_2 ($f_2 = 38.1$ mm), separated by a distance of 75 mm, focus the He–Ne beam down to a waist diameter of 40 $\mu\text{m} \pm 3$ μm . A single lens, L_3 ($f_3 = 100$ mm), focuses the excitation beam to a waist diameter of 40 $\mu\text{m} \pm 5$ μm . The method¹⁷ used for measuring these beam diameters was to translate a 10 μm pinhole, mounted in front of a photodiode, across the laser

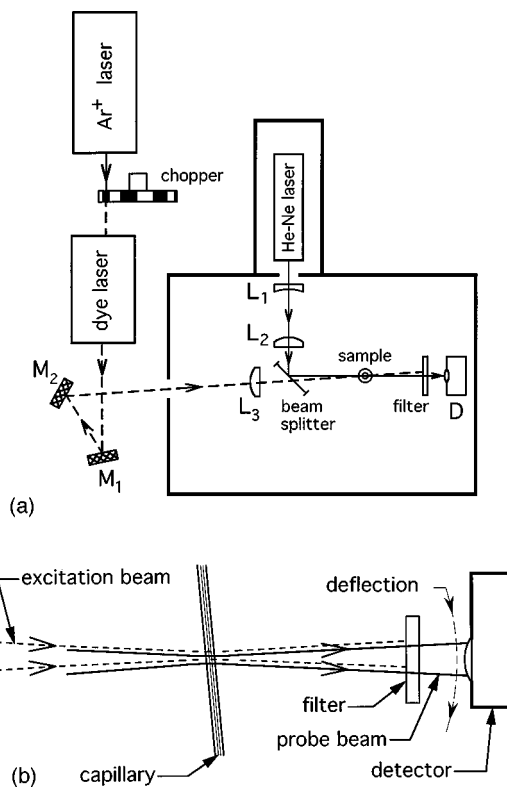


FIG. 1. (a) Plan view of apparatus. L_1 , L_2 , and L_3 , are lenses that focus the probe and excitation beams in the sample capillary, and D is a position sensitive detector. (b) Side view of focused optical beams overlapping within sample capillary.

beam. The spatial structure of each beam is close to that of a fundamental Gaussian mode. The beams intersect at their waists within a short (~ 10 cm) segment of a capillary (Polymicro Technologies model TSP 075375), having an external diameter of 375 μm and an internal diameter of 75 μm . The capillary material is the fused silica form of quartz. Its protective polyimide coating was removed with a razor blade, and the outer surface was cleaned with methanol and a lens tissue. The internal diameter of this capillary was chosen to be representative of those typically used for CE separations. Increasing the internal diameter would make optical measurements easier, but the specific constraints of a chemical separation process, e.g., heat dissipation, dictate what capillary size is practical. As the beams pass across the middle of the capillary, the curved walls act as a cylindrical lens, distorting the beams horizontally, but not vertically. The absence of vertical distortion facilitates a quantitative measurement of vertical deflection. Also, aligning the direction of deflection perpendicularly to the direction of optical distortion lessens the effect of capillary vibrations on the measurement. To a first order approximation, applying the lensmaker's formula¹⁸ to the curved surfaces of the capillary can provide a measure of the extent of horizontal distortion

$$\frac{1}{f_c} = 2 \left(\frac{n_c - 1}{r_o} + \frac{n_s - n_c}{r_i} \right). \quad (1)$$

In the above equation, f_c is the effective focal length (mm) of the cylindrical lens, and r_o and r_i are, respectively,

the outer and inner radii (mm) of the capillary. The term $n_c = 1.46$ is the refractive index of the quartz¹⁹ capillary material, and $n_s = 1.33$ is the refractive index of the aqueous sample. For the dimensions of the capillary used in this work, Eq. (1) gives $f_c = -0.49$ mm, indicating that the capillary forms a negative cylindrical lens. In PDS, minimal distortion is desired, so a capillary should be chosen such that the right-hand side of the equation is equal to zero. With a quartz capillary containing an aqueous sample, this occurs when the ratio of the capillary outer diameter to inner diameter is 3.5 to 1. However, even under such a condition, some distortion is inevitable, because the width of the optical probe beam is comparable to the width of the capillary column, causing significant off-axis lens aberration.

Before reaching the capillary, the two beams are incident on opposite sides of a dielectric 50% beamsplitter. The transmitted portion of the excitation beam and the reflected portion of the probe beam pass through the capillary at point S, overlapping each other within the capillary at an angle of 3° . This finite angle allows the beams to separate from each other, helping to prevent photothermal deflection from occurring outside the overlap region near the beam waists. On the opposite side of the 50% beamsplitter, the reflected portion of the excitation beam and the transmitted portion of the probe beam overlap in a symmetric manner. This second set of beams can be used differentially in conjunction with a reference cell for correction of background absorption.²⁰ However, because background absorption of the aqueous solvent in the experiments reported here was not a primary concern, these beams were not used. The capillary is tilted forward by about 5° , so that Fresnel reflections from the capillary walls do not go back into the HeNe laser. A narrow bandpass optical filter F (Newport Model 10 LF 01633) rejects stray light from the excitation beam and allows only the light from the probe beam to reach a position sensitive detector, D, located 20 cm beyond the capillary. The detector monitors vertical displacement of the probe beam spot.

We expected that measurement noise in the PDS system could originate primarily from four sources: (1) the pointing noise of the probe laser, (2) electronic noise, (3) convection or turbulence in the fluid media through which the probe beam passes, and (4) mechanical vibrations of optical components. Before conducting quantitative noise measurements, we incorporated features in the design of our apparatus to minimize each of these effects.

The pointing noise is inherent primarily in the probe laser itself, but also may be affected by the way that mounting hardware permits the laser head to cool. Our mount consists of two pillars, upon which the cylindrical laser head rests. Two fixed contact points on each pillar are made of a ceramic, chosen for low thermal conductivity. The surface area of the contacts is minimized. A nylon screw above each pillar applies downward pressure, fixing the position of the laser head. The intent of this design is to allow the head to cool uniformly, by both radiation and thermal contact with surrounding air.

In order to reduce electronic noise, we designed the position sensitive detector specifically for probe beam deflection measurements. It consists of a lens, two mirrors, and two

photodiodes, and has been described previously.²¹ The photodiodes are connected in parallel, with opposing polarities, thereby allowing a single low-noise current preamplifier (Stanford Research Systems Model SR570) to convert the photocurrents into a voltage which is proportional to the angular deflection of the probe beam. The amplified deflection signal is sent to a lock-in amplifier (Stanford Research Systems Model SR830), which can use the timing signal from the mechanical chopper as an external frequency reference.

Noise from convection currents was more likely to originate from laboratory air rather than from liquid within the capillary. An oscilloscope monitoring the deflection signal showed qualitatively that the wooden enclosure reduced low frequency fluctuations. As an added precaution against convective air currents, the enclosure contains a separate compartment with an aluminum lid for the HeNe laser, because the laser head generates a significant amount (~ 10 W) of heat. Small apertures in the walls of the enclosure allow the optical beams to enter the sample compartment. The barrier between the laser head and the sample also helps to maintain a stable sample temperature, which is important for PDS measurements.³ The temperature in the laboratory during our experiments was $23^\circ\text{C} \pm 1^\circ\text{C}$. Within the enclosure, the axes of the probe and excitation beams are 10 cm above the optical table, and the ceiling is 19 cm high.

To reduce noise from mechanical vibrations, optical components whose movements affect the deflection signal must be joined together in a dynamically rigid structure. For our apparatus, the critical components are the probe laser head, the two lenses that focus the probe beam, the beamsplitter, the capillary, and the detector. Where practical, we designed the mounting structures for these components so that the resonant frequencies for their modes of mechanical vibration would exceed the modulation frequency of the experiment. For example, the posts holding the two lenses and the beamsplitter were milled from solid cylinders of 6061-T6 aluminum, each with a diameter of 3.2 cm, and a height of about 11 cm. The base plates for these posts were fastened directly to the laser table (Newport model MST-410-8). For vibration analysis,²² it is appropriate to idealize each post as a uniform beam with one end cantilevered and the other end free. Using an elastic modulus of $E = 6.9 \times 10^9$ Pa, and a density of $\rho = 2.77$ g/cm³ for aluminum²³ gives a natural frequency of $f_n = 1850$ Hz for the fundamental mode of such a cylindrical beam. This value is greater than the modulation frequency that we expected to use. The pillar mounts for the HeNe laser head are shorter and thicker, and so their resonant frequencies are even higher. A nylon washer clamps the quartz capillary against an aluminum holder with a circular aperture, leaving an exposed span of 0.6 cm. Quartz¹⁹ has an elastic modulus of $E = 7.2 \times 10^9$ Pa, and a density of $\rho = 2.2$ g/cm³. Under the assumption that the exposed segment is cantilevered at both ends, vibration analysis gives that its fundamental resonant frequency exceeds 20 kHz.

Because the mounts for the two lenses, the beam splitter, and the He-Ne laser were fixed to the optical table, it was necessary that the positions of the capillary and the detector be made adjustable. For convenience, commercially available translation stages were selected for this purpose. The

capillary holder was mounted on a Newport model 466 three-axis translation stage,²⁴ and the detector was placed on a Newport model 462-XZ-M two-axis translation stage. The vibrational properties of these translation stages were not known. It was expected that the capillary holder might be susceptible to vibrations, because its translation stage uses flexure plates rather than roller bearings in its design. Although the flexure plates may be less dynamically rigid than roller bearings, they were chosen because they allow for smooth motion and fine adjustment of the sample.

III. NOISE MEASUREMENTS

To characterize our apparatus, we placed an aqueous sample, of 1×10^{-3} M NdCl_3 dissolved in 1×10^3 M HCl , in the capillary and measured the inherent noise in the system with the excitation beam turned off. For these initial noise measurements, it was necessary only that the sample be transparent to the probe beam. In other respects, its spectral properties were not important. The current preamplifier gain was 10^6 V/A. A desktop computer program used the following algorithm to control the lock-in amp and to calculate the noise: (1) The computer commands the lock-in amp to use its internal timing mechanism (rather than an external reference signal) to allow it to function as a narrow bandpass filter at a specified initial frequency. (2) After waiting for the duration of one time constant, the computer queries the lock-in for the “in-phase” and “quadrature” values of the deflection signal. Each of these values represents a scalar quantity that corresponds to one of the two orthogonal components of a periodic signal. (3) The computer repeats step (2) many times, accumulating a sequence of data points for a single frequency. (4) The computer calculates the standard deviation in the accumulated data, using the corrected two-pass algorithm.²⁵ (5) The “noise” at each frequency is defined as half the sum of the standard deviations for the in-phase and for the quadrature, divided by the square root of the effective noise bandwidth (ENBW) of the lock-in amp. For this calculation, the time constant and the number of “poles” in the low-pass filter stage of the lock-in amp determine the ENBW. As the number of accumulated data increases, the standard deviation of the in-phase should approach that of the quadrature, because the reference signal originates from an internal clock, asynchronously from any external physical process. This is the noise that a single channel of the lock-in amp will incur when the lock-in uses an external frequency reference. (6) The program writes the computed data into a file. (7) The internal frequency setting is increased incrementally, and steps (2)–(6) are repeated. This procedure continues until a specified final frequency is reached.

Figure 2 shows a scanned measurement of noise in the apparatus as a function of frequency, from 10 to 400 Hz. Noise is displayed in both angular and electrical units. The time constant of the lock-in was 0.3 s, with a two-pole (12 dB/octave) low-pass filter, for an ENBW of 0.4167 Hz. To calculate each value of noise on the figure, the program accumulated a sequence of 500 queries from the lock-in. The frequency increment was 0.5 Hz between measurements. The graph shows that, for frequencies below 100 Hz, there are

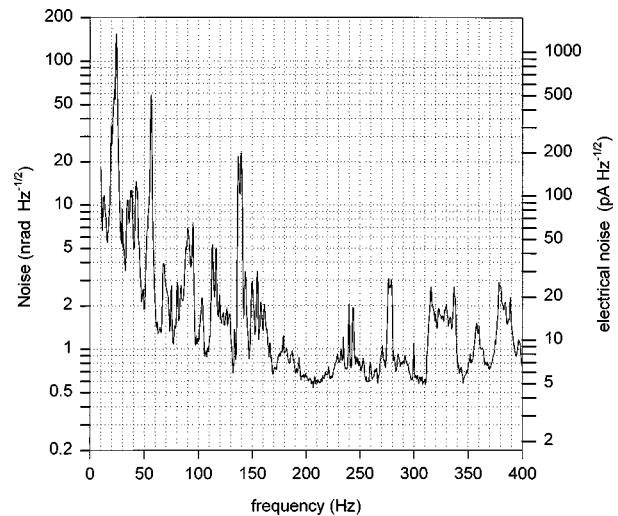


FIG. 2. Deflection noise as a function of frequency with an aqueous sample in place.

several noise peaks superimposed upon an apparent $1/f$ trend. Although the peak just below 140 Hz may be associated with the fundamental vibrational mode of the optical table, we believe that most of the low frequency noise originates from pointing fluctuations within the laser head. Noise with a $1/f$ trend is generally called “flicker noise” or “pink noise,” and often arises in electronic circuits when a voltage is applied across a resistor.²⁶ This $1/f$ electronic noise occurs because of fluctuations in electrical resistance. The mechanism of $1/f$ pointing noise in the laser head may be comparable to that of electrical noise in a resistor, except that its origin is thermal rather than electrical. In a resistor, the applied voltage causes current to flow, inducing fluctuations in resistance which appear as electronic noise. In the He–Ne laser head, the thermal power originating internally from the plasma causes heat to pass through the outer walls of the plasma tube, inducing temperature fluctuations. Because of thermal expansion of the plasma tube material, these fluctuations may alter the alignment of the laser mirrors, appearing as pointing noise.

For PDS experiments, the most favorable frequency domain appears to be 195–220 Hz, where the measured noise level, in units of current, remained fairly constant, at a level just above $5.1 \text{ pA Hz}^{-1/2}$, which corresponds to an angular deflection noise of $0.6 \text{ nrad Hz}^{-1/2}$. We attribute this noise floor to photodiode shot noise. In the measurement of current from a single photodiode, the commonly used formula for shot noise, I_s ($\text{A Hz}^{-1/2}$), is

$$I_s = \sqrt{2eI}, \quad (2)$$

where $e = 1.6 \times 10^{-19}$ C is the charge of an electron, and I is the photocurrent produced (A). In estimating the shot noise for the position sensitive detector with two photodiodes, we use the sum of photocurrents produced. To evaluate these, we reduced the gain of the current preamplifier and alternately masked the upper and lower halves of the detector, obtaining a figure for the sum of the photocurrents to be $74 \text{ } \mu\text{A}$. This value in the preceding formula implies that shot noise should have been $4.9 \text{ pA Hz}^{-1/2}$, which is consistent

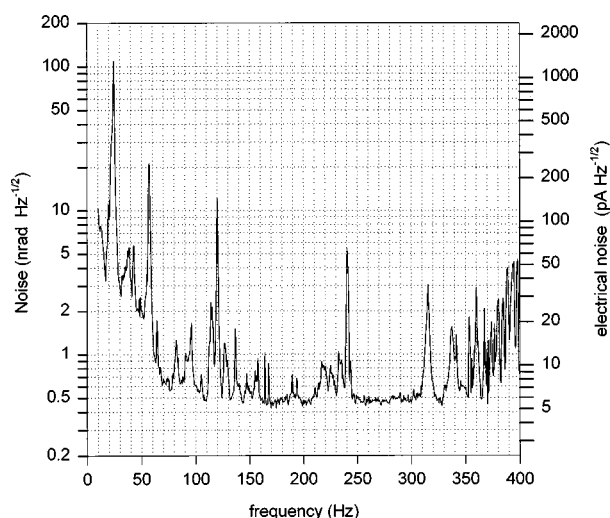


FIG. 3. Deflection noise as a function of frequency with the sample capillary removed.

with the measured noise. The combined internal electrical noise of the current preamp and the lock-in amp was less than $1 \text{ pA Hz}^{-1/2}$, so photodiode shot noise dominates.

From observations on an oscilloscope, it was apparent that lightly tapping the translation stage that holds the capillary seemed to induce significant vibrations, which affected the vertical deflection signal. Ideally, perturbations in the capillary position should cause horizontal, rather than vertical, deflections of the probe beam. The observed deflections probably occur because of microscopic irregularities in the capillary and because of misalignment of the axis of the position detector with respect to the capillary axis. It is also possible that some probe beam radiation is scattered from the capillary and refocused by lenses L_2 and L_1 back into the He-Ne laser cavity, thereby causing probe beam output noise when the capillary vibrates. Under normal conditions in the laboratory, external vibrations can be transferred to components on the optical table either mechanically through the table legs, or acoustically through the air. To check the effect of capillary vibrations on deflection noise, we removed the capillary from the path of the probe beam, and repeated the previous noise measurements. To reduce the measurement time, the number of records for each statistical noise calculation was decreased from 500 to 400. Other parameters remained the same. Figure 3 shows the results of this test, with features similar to those of the previous measurements. A notable difference is that the “white” shot noise floor is more clearly visible, particularly in the frequency domain of 250–310 Hz. This indicates that capillary vibrations may contribute significantly, although their intermittent nature makes numerically evaluating the magnitude of their effect difficult. By eliminating optical losses due to distortion and Fresnel reflections, removal of the capillary increased the photocurrents in the detector to 83 pA. This increased the electrical shot noise, which scales linearly with \sqrt{I} , to $5.2 \text{ pA Hz}^{-1/2}$. However, the responsivity of the detector (in units of A/rad) scales linearly with I . Therefore, the effect of shot noise upon angular measurement (in units of $\text{rad Hz}^{-1/2}$) decreased, scaling linearly with $1/\sqrt{I}$. In the domain of 195–

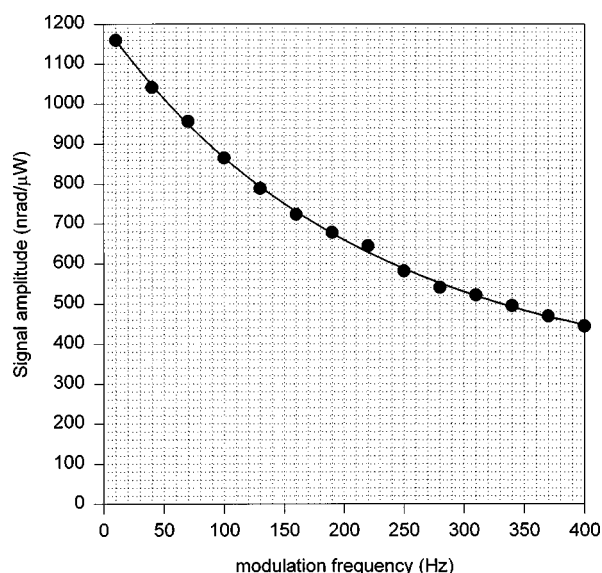


FIG. 4. Deflection amplitude as a function of modulation frequency. Normalization is with respect to the absorbed excitation power.

210 Hz, capillary removal reduced the observed deflection noise to below $0.5 \text{ nrad Hz}^{-1/2}$. Other changes in noise peaks above the shot noise floor, e.g., in the range of 300–400 Hz, probably occurred because intermittent environmental disturbances differed between the two noise measurement scans.

IV. PERFORMANCE OF APPARATUS

In order to determine the optimal modulation frequency for our apparatus, we performed a sequence of photothermal deflection measurements at a fixed optical wavelength, varying the modulation frequency from 10 to 400 Hz, at 30 Hz increments. The capillary contained the solution of $1 \times 10^{-3} \text{ M NdCl}_3$ in $1 \times 10^{-3} \text{ M HCl}$. The dye laser was tuned to the center of the Nd^{3+} absorption peak, at 575 nm. The molar absorptivity of Nd^{3+} at this wavelength is $6.9 \text{ M}^{-1} \text{ cm}^{-1}$, so the optical absorbance through the middle of the $75 \text{ }\mu\text{m}$ circular cross section of the sample is 5.2×10^{-5} . The output mirror of the dye laser is wedge shaped rather than uniformly thick, so that the Fresnel reflection of the primary output beam from its uncoated outer surface will not be directed straight back into the laser cavity. From this reflection, the laser emits a less powerful secondary output beam, which deviates at an angle from the primary beam. We captured this secondary beam with a radiometrically corrected photodiode, for normalization of measurements with respect to output power. The focusing lens, L_3 , for the primary excitation beam was mounted on a Newport model 461-XYZ-M three-axis translation stage. We adjusted the position of this lens to obtain maximum deflection amplitude for each modulation frequency. A maximum occurs where the excitation beam is either slightly above or slightly below the probe beam. By observing the difference in lens position for these two maxima, we could deduce a value for the optimal vertical offset between the beams. This vertical offset varied from $\pm 27 \text{ }\mu\text{m}$ at 10 Hz, to $\pm 17 \text{ }\mu\text{m}$ at 400 Hz. The measured amplitude values appear as individual data points in Fig. 4, showing that signal amplitude monotonically de-

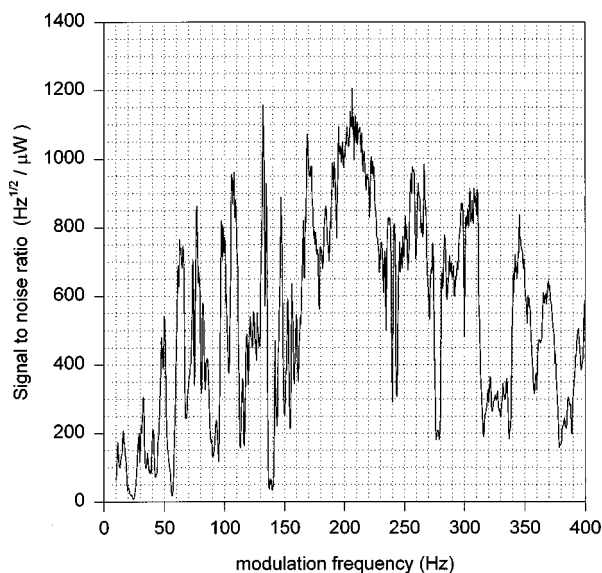


FIG. 5. Signal-to-noise ratio as a function of modulation frequency, as calculated by dividing the data of Fig. 4 by that of Fig. 2. SNR units account for the effective noise bandwidth of the lock-in amplifier and the power of the absorbed radiation.

creases with increasing modulation frequency. Incidentally, the phase lag of the deflection signal for the points of optimal alignment varied from 7° at 10 Hz, to 60° at 400 Hz. The experimental data seem to conform to expectations³ based on the principles of thermal diffusion. For very low frequencies, the thermal conductivity (W/cm K) of the sample and capillary materials dominate thermal diffusion. In this low frequency limit ($f \rightarrow 0$), the signal amplitude approaches a constant value, and the phase lag approaches zero. For very high frequencies, the product of heat capacity (J/g K) times the density (g/cm³) of the sample dominates thermal diffusion. In this high frequency limit ($f \rightarrow \infty$), the signal amplitude asymptotically approaches a line proportional to $1/f$, and the phase lag approaches 90° . Our data lie in-between these two limits. We matched the amplitude data to a continuous curve, using a least-squares fit to a fourth-degree polynomial in f . The continuous curve fit is shown, along with the individually measured data points, in Fig. 4.

We divided the polynomial fit of Fig. 4 by the data of Fig. 2, to compute the signal-to-noise ratio (SNR) as a function of modulation frequency. Figure 5 shows the results, expressing SNR in units of $\text{Hz}^{1/2}/\mu\text{W}$. For a specific set of experimental conditions, SNR can be expressed in its more traditional form as a dimensionless quantity, depending on the absorbed excitation power and the ENBW of the electronic filtering system. Multiplying a data point from Fig. 5 by the absorbed excitation power (in μW), and dividing by the square root of ENBW (in $\text{Hz}^{1/2}$), will achieve this result. SNR is maximized, at a level above $1000 \text{ Hz}^{1/2}/\mu\text{W}$, for a frequency domain near 205 Hz, so we choose for spectral scans to modulate the excitation beam at this frequency. Increasing the modulation frequency above the measured domain of Fig. 5 would not improve SNR, because signal amplitude would continue to decrease, while noise could not decrease below the white shot noise floor.

As a demonstration of the ability of our apparatus to

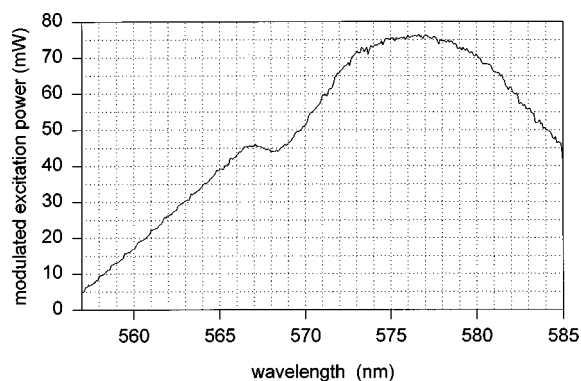


FIG. 6. Incident excitation beam power as a function of wavelength. The beam is chopped with a 50% duty cycle, at a rate of 205 Hz. The rms modulated power shown is equal to one half of the peak power.

obtain an optical absorption spectrum, we used a stepper motor (Oriel model 18510) to scan the wavelength of the dye laser at a constant rate of 0.155 nm/s. The lock-in amp was set to measure the in-phase component of a signal with a phase lag of 43° . The time constant was 0.3 s, with a two-pole (12 dB/octave) low-pass filter. The amplified photodiode signal was fed through a Stanford Research Systems Model SR235 analog processor, which acted as a single-pole (6 dB/octave) low-pass filter with a 0.3 s time constant. During the scan, the computer recorded the lock-in deflection signal components and the filtered normalization data at 0.5 s intervals. Figure 6 shows the output power of the dye laser during the scan, and Fig. 7 shows a normalized spectrum of the $1 \times 10^{-3} \text{ M Nd}^{3+}$ solution. The spectrum clearly shows the characteristic absorption peak of neodymium, although we believe that two effects may have increased noise levels during the scan above those that we had measured previously. The first is mechanical vibration caused by the step motor used for scanning the dye laser. Because all optical components directing the probe beam are attached to the same structure as the dye laser, the mechanical disturbances can create significant noise. The second effect is fluctuation in the output of the dye laser. Ideally, power fluctuations do not cause noise directly, but the amplitude of the signal

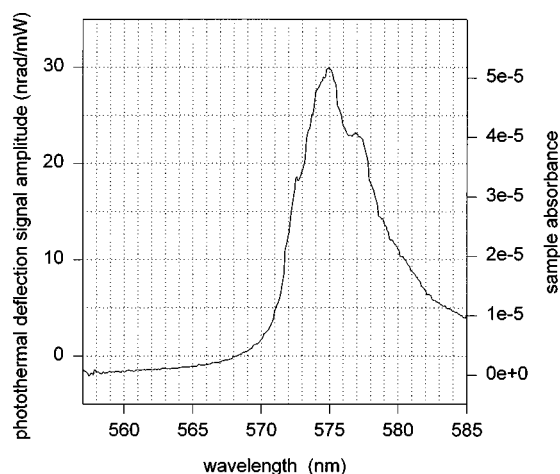


FIG. 7. Photothermal deflection spectrum of a $1 \times 10^{-3} \text{ M Nd}^{3+}$ aqueous solution in a $75 \mu\text{m}$ internal diameter silica capillary. Normalization is with respect to incident excitation power.

should vary in direct proportion to the power. If the filter on the normalization channel has exactly the same temporal response as the lock-in amp low-pass filter, then the power fluctuations should not affect the normalized measurement. However, because there is some difference in these, an unsteady excitation beam can result in measurement error that appears as noise. Also, changes in the alignment or the wavelength of the excitation beam can cause similar unsteadiness in the measured deflection amplitude.

An interesting feature of the spectrum of Fig. 7 is that the base line goes slightly below zero for optical wavelengths near 560 nm, away from the Nd^{3+} absorption peak. We attribute this to photothermal deflection occurring within the silica capillary material rather than in the liquid sample. The thermo-optic coefficient, dn/dT , of fused silica²⁷ is $8.7 \times 10^{-6} \text{ }^\circ\text{C}^{-1}$, whereas for water³ at 25 $^\circ\text{C}$, $dn/dT = -1.038 \times 10^{-4} \text{ }^\circ\text{C}^{-1}$. Because the sign for dn/dT of the capillary material is opposite that of the sample, background absorption from external surface contamination or from bulk absorption in the fused silica appears as a negative deflection amplitude. In Fig. 7, this background offset is equal to about -2 nrad/mW , a deflection comparable in magnitude to that observed from a sample with an optical absorbance of 4×10^{-6} . A calibrated absorbance scale for the spectrum is shown as a second vertical axis.

In the initial setup of the apparatus, absolute cleanliness of the optical surfaces was not our primary concern. However, Fig. 7 shows that the effects of surface contamination can be significant. To further illustrate these effects, we intentionally translated the capillary vertically until the excitation beam was incident upon a spot that was less clean, and scattering of both optical beams from the capillary was apparent. We repeated the spectral scan, and plotted the new data in Fig. 8. Here, the photothermal deflection signal from the speck of contaminant dominates, causing a signal offset in excess of -50 nrad/mW . Although noise is significantly increased, the Nd^{3+} absorption peak is still easily discernible, with a height close to that of the previous spectrum. The optical flaws introduced by the surface contaminant may increase noise by sensitizing the deflection signal to capillary vibrations, or by increasing the amount of optical radiation that is scattered back into the He-Ne laser head. Also, the background signal from the surface contaminant may be particularly sensitive to drift in the alignment of the excitation beam.

With the optical beams overlapping at an angle of 3° , their axes diverge from one another in the horizontal direction by only $2 \text{ } \mu\text{m}$ at the inner wall of the capillary, and by only $10 \text{ } \mu\text{m}$ at the outer wall. These values are less than the beam radii, and also less than the thermal diffusion length, which is a measure of the extent to which periodic thermal gradients travel in a material. The thermal diffusion length is defined as $\sqrt{\kappa/\rho C_p \pi f}$, where κ is the thermal conductivity, ρ is the density, C_p is the heat capacity, and f is the modulation frequency expressed in Hz. At 205 Hz, the thermal diffusion lengths in water and quartz are 15 and 36 μm , respectively. One way of reducing the unwanted mirage effect within the capillary wall would be to increase the overlap angle of the optical beams, perhaps aligning them per-

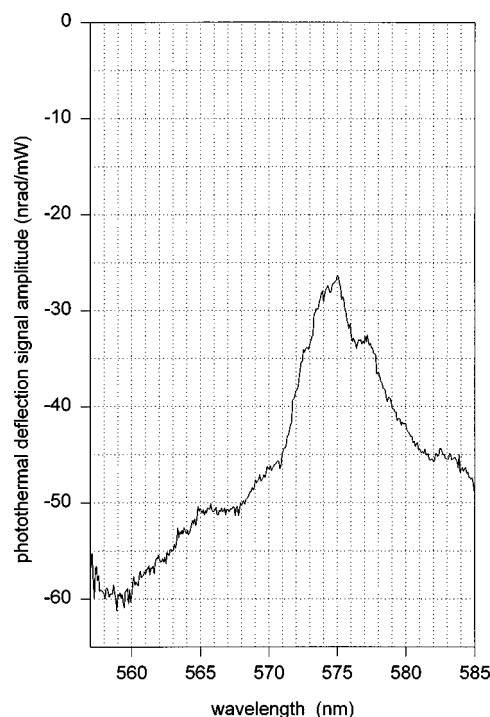


FIG. 8. Photothermal deflection spectrum of a $1 \times 10^{-3} \text{ M Nd}^{3+}$ aqueous solution in a $75 \text{ } \mu\text{m}$ internal diameter silica capillary, with contamination on the outer surface of the capillary.

pendicularly, as in previously reported^{12,13} thermal lensing measurements. Although such a transverse arrangement would cause an unwanted decrease in signal amplitude, the benefit of background signal reduction might be worthwhile in some situations.

V. DISCUSSION

As the first reported application of PDS within a micrometer-bore capillary, our apparatus successfully demonstrates the applicability of this technique to capillary electrophoresis separations. Our work shows that, with careful precautions and systematic noise measurements, it is possible to reduce the effect of mechanical disturbances until photodiode shot noise is the predominant source of noise. Although the background signal due to photothermal deflection within the quartz capillary wall is an important consideration, the clear resolution of spectra from dilute samples is possible, even without absolute cleanliness of the capillary exterior.

In assessing the ultimate sensitivity of an analytical technique, it is customary to quote a value for the limit of detection (LOD). An accepted definition²⁸ for the LOD is the concentration of analyte for which the SNR is equal to 3. Our work has emphasized the limitations arising from noise in the measurement of deflection. Ideally, increasing the time constant of the lock-in amplifier can reduce the effect of this noise indefinitely, because the ENBW is inversely proportional to the time constant. Similarly, increasing the available power from the excitation beam will improve SNR, as long as the deflection signal is linearly proportional to the excitation power. However, in a practical experiment involving a capillary electrophoresis separation, the time available for measurement is limited, as is the available power output

from a cw laser source. Also, problems that are not alleviated by increased noise filtering may exist in a real experiment.

We believe that, apart from noise, the most important problems in the practical application of photothermal deflection spectroscopy to trace detection can generally be classified as signal drift. Signal drift can become especially important when the signal due to sample absorption decreases to less than the signal due to background absorption. Although the background signal due to photothermal deflection in the capillary wall may be important, the technique of capillary electrophoresis helps reduce the effect of solvent background absorption, because the separated sample ions are locally concentrated in the column. Signal drift due to temperature variation is particularly important in PDS, primarily because the material parameter, dn/dT , is dependent upon temperature. For this reason, ultimate sensitivity may require careful temperature maintenance. Another form of drift is due to changes in the alignment or mode structure of the excitation beam. Extending the time of measurement can reduce noise, but it may actually aggravate the problem of signal drift.

To calculate the LOD of our system, we will use as an example the experimental conditions for the spectrum of Fig. 7, along with the measured noise from Fig. 2. For such a computation, it is necessary to assume that the problems of background absorption and drift have been sufficiently addressed so that signal amplitude and noise determine the LOD. At the absorption peak of Nd^{3+} , the available power was 75 mW, and the lock-in amp used a 12 dB/octave, 0.3 s time constant. For a signal-to-noise ratio of 3 at the limit of detection under these conditions, the minimum detectable absorbance would be $A = 2.4 \times 10^{-8}$, which translates into an absorption coefficient of $\alpha = 3.2 \times 10^{-6} \text{ cm}^{-1}$, or a Nd^{3+} concentration of $4.6 \times 10^{-7} \text{ M}$.

The results from our apparatus compare favorably with those reported from other techniques, and adjustments to our initial design could enhance performance even further. A logical improvement would be to reduce the effect of probe beam shot noise by increasing the photocurrent. For example, a sharply edged mirror could replace the 50% beam-splitter, so that the probe beam would reflect off an area of the mirror near the edge, and the excitation beam would pass straight by the edge of the mirror. This sort of arrangement would double both the photocurrent and the excitation power incident on the sample, thereby improving SNR by up to a factor of $2\sqrt{2}$. Also, further isolating the probe beam optical components from the effect of mechanical vibrations would be beneficial. A simple step would be to replace the translation stage that holds the capillary with a more dynamically rigid device. A more thorough method²⁹ of vibration isolation is to mount the sample and the probe beam optical components on a compact rigid platform rather than directly on the laser table. Foam rubber pads or some other soft material can support the platform on the optical table, thereby providing vibration isolation.

Also, it may be worthwhile to focus the optical beams down to smaller waist diameters in the capillary. Because the intensity of a laser beam at its center is inversely proportional to the square of its diameter, shrinking the excitation beam would increase the amplitude of local temperature

fluctuations (in units of degrees K). The reduced size of the excitation beam also would dictate that these increased temperature fluctuations would be confined to a smaller region, further increasing the magnitude of the temperature gradient (in units of K/cm). The disadvantage of reducing the size of the optical beams is that the far-field diffraction angle would increase, being inversely proportional to the waist diameter. Even though the beams do not expand significantly within the sample capillary, the size of the probe beam spot incident on the position sensitive detector would increase. Because the responsivity of a bi-cell-type position sensor to vertical displacements (in units of A/cm) is inversely proportional to the height of the spot, this effect of increased diffraction would tend to decrease the amplitude of the electronic signal. Thus, a trade-off exists between the benefit of increasing the thermal gradients and the detriment of reducing the electrical responsivity. Proper consideration of these effects may lead to improved performance in the development of a future design.

ACKNOWLEDGMENTS

This work was funded by the U.S. Department of Energy's Nonproliferation and National Security Program, Office of Research and Development (NN-20) and was performed under the auspices of the Department of Energy by Lawrence Livermore National Laboratory under Contract No. W-7405-ENG-48.

- ¹W. B. Jackson, N. M. Amer, A. C. Boccarda, and D. Fournier, *Appl. Opt.* **20**, 1333 (1981).
- ²G. R. Long and S. E. Bialkowski, *Anal. Chem.* **58**, 80 (1986).
- ³J. D. Spear, R. J. Silva, G. L. Klunder, and R. E. Russo, *Appl. Spectrosc.* **47**, 1580 (1993).
- ⁴S. E. Bialkowski, *Photothermal Spectroscopy Methods for Chemical Analysis* (Wiley, New York, 1996).
- ⁵J. W. Jorgenson and K. D. Lukacs, *Science* **222**, 266 (1983).
- ⁶*Handbook of Capillary Electrophoresis: Theory and Practice*, edited by J. P. Landers (CRC, Boca Raton, FL, 1994).
- ⁷R. Weinberger, *Practical Capillary Electrophoresis* (Academic, San Diego, CA, 1993).
- ⁸R. L. St. Claire, *Anal. Chem.* **68**, R569 (1996).
- ⁹D. J. Bornhop, and N. J. Dovichi, *Anal. Chem.* **59**, 1632 (1987).
- ¹⁰A. E. Bruno, A. Paulus, and D. J. Bornhop, *Appl. Spectrosc.* **45**, 462 (1991).
- ¹¹T. Odake, T. Kitamori, and T. Sawada, *Anal. Chem.* **67**, 145 (1995).
- ¹²M. Yu and N. J. Dovichi, *Anal. Chem.* **61**, 37 (1989).
- ¹³K. C. Waldron and N. J. Dovichi, *Anal. Chem.* **64**, 1396 (1992).
- ¹⁴J. Wu, T. Kitamori, and T. Sawada, *Anal. Chem.* **62**, 1676 (1990).
- ¹⁵J. Wu, T. Odake, T. Kitamori, and T. Sawada, *Anal. Chem.* **63**, 2216 (1991).
- ¹⁶T. Odake, T. Kitamori, and T. Sawada, *Anal. Chem.* **64**, 2870 (1992).
- ¹⁷D. Letalick and I. Renhorn, *Rev. Sci. Instrum.* **58**, 765 (1987).
- ¹⁸J. D. Spear, R. E. Russo, J. E. Andrews, and P. M. Grant, *Rev. Sci. Instrum.* **63**, 4457 (1992).
- ¹⁹*CRC Handbook of Chemistry and Physics*, 75th ed., edited by D. R. Lide (CRC, Boca Raton, FL, 1994).
- ²⁰J. D. Spear, R. E. Russo, and R. J. Silva, *Appl. Spectrosc.* **42**, 1103 (1988).
- ²¹J. D. Spear and R. E. Russo, *Rev. Sci. Instrum.* **67**, 2481 (1996).
- ²²L. S. Jacobsen and R. S. Ayre, *Engineering Vibrations* (McGraw-Hill, New York, 1958), Chap. 10, pp. 492-496.
- ²³E. R. Popov, *Introduction to Mechanics of Solids* (Prentice-Hall, Englewood Cliffs, NJ, 1968), p. 554.
- ²⁴This model is no longer manufactured. A comparable device is now sold by Thorlabs, as model MDT616.
- ²⁵W. H. Press, S. A. Teukolsky, W. T. Vetterling, and B. P. Flannery, *Nu-*

merical Recipes in FORTRAN: The Art of Scientific Computing, 2nd ed. (Cambridge University Press, New York, 1992), Chap. 14, pp. 604–609.

²⁶P. Horowitz and H. Hill, *The Art of Electronics*, 2nd ed. (Cambridge University Press, New York, 1989), Chap. 7, p. 432.

²⁷R. M. Waxler and G. W. Cleek, *J. Res. Natl. Bur. Stand.* **77A**, 755 (1973).

²⁸G. L. Long and J. D. Winefordner, *Anal. Chem.* **55**, 712A (1983).

²⁹Z. Y. Deng, J. D. Spear, J. D. Rudnicki, F. R. McLarnon, and E. J. Cairns, *J. Electrochem. Soc.* **143**, 1514 (1996).